Indian Journal of Chemical Technology
Vol. 30, July 2023, pp. 534-546
DOI: 10.56042/ijct.v30i4.69826

Pulsatile flow of Jeffrey hybrid nanofluid in a vertical channel with entropy generation

A Subramanyam Reddy & T Thamizharasan*

Department of Mathematics, School of Advanced Sciences, Vellore Institute of Technology, Vellore-632 014, Tamil Nadu, India

*E-mail: tamilarasan962@gmail.com

Received 23 December 2022; accepted 6 April 2023

This study examines the hydrodynamic pulsatile flow of Jeffrey hybrid (Au+Al_2O_3/Blood) nanofluid in a vertical channel with entropy production. The literature shows that the investigations are only related to the pulsating flow of nanofluid. Any study related to the pulsating flow of Jeffrey hybrid nanofluid in a vertical channel with Joule heating, thermal radiation, and heat source/sink did not report so far. The novelty of the present work is the investigation of entropy generation on pulsatile flow of Jeffrey hybrid nanofluid with Joule heating, thermal radiation and heat source/sink effects in a vertical channel. The transformation of the governing partial differential equations into a system of ordinary differential equations are made by applying the perturbation method and then numerically solved by fourth-order Runge-Kutta method aided by bvp4c shooting technique built-in MATLAB software. This work is useful for chemical engineering, blood cancer treatment, nano-drug delivery, pharmaceutical process, and biomedical aspects.The effects of various emerging parameters and variables on velocity, temperature, entropy generation, and the Bejan number are displayed through graphs. The consequences of physical parameters on heat transfer rate are prearranged in a table. This analysis demonstrates that the temperature of hybrid nanofluid increases with an increment in radiation parameter, and Eckert number. The entropy generation is an increasing function of Eckert number and radiation parameter whereas it decelerates with a rise in Hartmann number. The heat transfer rate has a higher impact in the case of (Au+Al_2O_3/Blood) hybrid nanofluid as compare to mono nanofluid.

Keywords: Entropy generation, Jeffrey hybrid nanofluid, Pulsatile flow, Vertical channel, Grashof number

In recent years, researchers have been increasingly focusing on pulsatory flows in a channel or pipe, due to their significance in both biological and industrial purposes, such as in pulse jets, drying technology, internal combustion engines, packed-bed heat exchangers, and so on [1-8]. Kot *et al.*[9] numerically observed the unsteady pulsatile non-Newtonian fluid flow over a vertical stenosed artery with stress and strain fractional parameter effects by implementing Laplace and finite Hankel transformations. Eldabe and Zeid[10] inspected the MHD pulsatile non-Newtonian fluid flow between two porous vertical plates in the existence of Ohmic heating, Eckert number, and radiation effects by implementing the homotopy perturbation technique. Pant *et al.*[11] scrutinized the pulsatile laminar flow in a two parallel plates with time dependent thermal boundary conditions by applying the finite volume method. Maskeen *et al.*[12] reported the impression of Joule heating on pulsatile solid-liquid flow on a concentric cylinder in a permeable medium by utilizing the Runge-Kutta-Fehlberg fourth-fifth-order numerical technique. Haq *et al.*[13] reported hydromagnetic pulsatory carbon nanofluid flowing between two concentric cylinders with the effect of Reynolds number and Hartmann number. Shah *et al.*[14] explored the magnetic field effect on pulsatile blood flow over an inclined porous cylindrical tube by using the Laplace transformation method. Wang *et al.*[15] considered the oscillating flow of blood and heat transfer via small vessels along with radiative heat and Ohmic heating consequences by executing the finite difference method.

Recently, many researchers have more interested in studying nanofluids in various configurations due to their widespread applications. The formation of a hybrid nanofluid is characterised by the addition of two or more distinct nanoadditives to the base fluid. Hybrid nanofluids have a wide range of potential uses in nearly every field of industrial and engineering such as heat exchanger, electronics, automotive, refrigeration sectors and so on [16-30]. Abbas *et al.*[31] evaluated the Cu-water nanofluid in a square cavity with two barriers under the existence of Hartmann number by utilizing the Galerkin finite element method. Ahmed *et al.*[32] scrutinized the hydromagnetic Eyring-Powell nanofluid

flow in a moving/static wedge with the influence of thermal radiation. The hydrodynamic non-Newtonian nanofluid flow on an exponentially permeable stretchy surface with heat source and sink by using bvp4c technique was studied by Li *et al.* [33]. Abbasi *et al*. [34] studied the peristaltic flow of blood based hybrid nanofluid in a curved channel by using Reynolds model approach with Hall effect and magnetic field. A finite difference technique was used to study the consequence of radiative heat and heat generation/absorption on water conveying hybrid nanofluid on a stretching sheet by Hussain *et al.*[35]. Iftikhar *et al.* [36] elaborated the hydromagnetic flow of hybrid ($Cu+SiO_2$)/water nanoliquid through a non-uniform tube by utilizing Cauchy's Euler's technique. Elsaid and Abdel-wahed[37] recognized the thermal radiation impact on hybrid $Cu+Al_2O_3$/water nanofluid passing in a vertical channel.

In recent years, there has been considerable progress in studying non-Newtonian fluid flow. Oils, paints, ketchup, and fluid polymers are examples of non-Newtonian fluids. Non-Newtonian models are classified into the following three subcategories: integral, differential, and rate. Among such models one is Jeffrey fluid which belongs to the category of non-Newtonian fluids of rate type. Jeffrey model deals with retardation time and the ratio of relaxation time to retardation time [38-42]. Saif *et al.*[43] scrutinized the heat source and sink consequences on Jeffrey nanoliquid flow passing over an extendable curved sheet. Aleem *et al.*[44] analytically observed the impressions of Grashof and Hartmann number on hydrodynamic Jeffrey fluid in a vertical channel by using the Laplace transform scheme. Ali *et al.*[45] inspected the hydromagnetic flow of hybrid (TiO_2+Cu/H_2O) nanoliquid through an asymmetric channel under the influence of pressure gradient and Eckert number by employing the Adams-Bashforth scheme. Hafeez *et al.*[46] scrutinized the Jeffrey-Hamel hybrid nanofluid flow in a convergent/divergent channel incorporating Reynolds number and magnetic field effects.

Entropy is the amount of energy created by irreversible processes in a thermal system. It has been discovered that such thermal energy can not be put to any good use. As a result, minimizing entropy is beneficial for increasing the performance of the thermal system[47-52]. Hayat *et al.*[53] scrutinized the entropy production with viscous dissipation, Ohmic heating, and radiative heat effects on hydromagnetic Jeffrey nanoliquid flow on an extendable sheet. Mansour *et al.*[54] hydromagnetic flow of water conveying hybrid (Cu and Al_2O_3) nanoliquid through a square cavity in the existence of entropy generation by implementing finite difference method. Entropy analysis on Jeffrey nanoliquid flow passes a variable thickened surface with Ohmic heating and nonlinear radiative heat flux is explored by Javed *et al.*[55]. Li *et al*. [56] analysed entropy distribution on the radiative time dependent flow through an infinite plate with the existence of Joule heating, viscous dissipation by implementing finite difference method. Hussain *et al.*[57] used the finite element scheme to study the entropy production on hybrid nanofluid flow along a horizontal channel with a square obstacle.

The primary purpose of this study is to analyze the impact of thermal radiation, Eckert number and heat source/sink on pulsatile flow of Jeffrey hybrid ($Au+Al_2O_3$/Base fluid) nanoliquid between two parallel vertical walls with entropy generation. The governing equations are transformed to a system of ordinary differential equations by applying the perturbation procedure then numerically tackled with the fourth-order Runge-Kutta scheme aided by the shooting method. The consequences of various physical parameters and variables on velocity, temperature, entropy generation, and Bejan number are presented graphically. A hybrid ($Au+Al_2O_3$)/ blood nanofluid provides a higher heat transfer rate compared to a mono nanofluid. The heat transfer rate (Nusselt number) is tabulated for various values of emerging parameters are examined in detail.

Formulation of the problem

The values of thermophysical properties of nanoparticles (Au, Al_2O_3) and base fluid (blood) are given in Table 1. This current flow problem deals with the pulsating flow of laminar and incompressible electrically conducting non-Newtonian Jeffrey hybrid nanoliquid between two parallel vertical walls. The flow geometry of the model is presented in Fig. 1 shows that the left wall runs parallel to the

Table 1 — The values of thermophysical properties of nanoparticles (Au, Al_2O_3) and base fluid (blood)[3,16,35]

Property	Blood	Au	Al_2O_3
$\rho\,(kg/m^3)$	1053	5200	3970
$C_p\,(J/kg/K)$	3594	670	765
$K\,(W/mK)$	0.492	6	40
$\sigma(\Omega m)^{-1}$	0.8	25000	$1x10^{-10}$

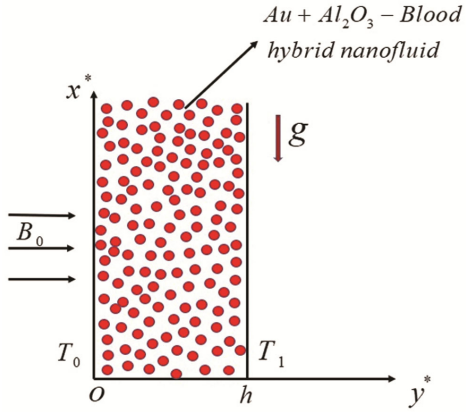

Fig. 1 — Schematic sketch of the problem

x^*-axis, while y^*-axis runs perpendicular to the walls, h indicates hight between the plates. B_0 symbolizes intensity of magnetic field is applying orthogonal to the flow direction. $T_1 (> T_0)$ and T_0 are the temperatures of the right and left walls. Let us consider that the pulsating flow is induced by the pressure gradient for the present study is expressed as [1,2,9]

$$-\frac{1}{\rho_f}\frac{\partial P^*}{\partial x^*} = A(1+\varepsilon e^{i\omega t^*}), \qquad \ldots(1)$$

here t^* is dimensional time, ω is frequency, P^* is the dimensional pressure, $\varepsilon (<< 1)$ is suitably chosen positive quantity, A is constant.

By these assumptions the governing equations are,

$$\rho_{hnf}\frac{\partial u^*}{\partial t^*} = -\frac{\partial P^*}{\partial x^*} + \frac{\mu_{hnf}}{1+\lambda_1}\frac{\partial^2 u^*}{\partial y^{*2}} - \sigma_{hnf}B_0^{\,2}u^* + \frac{\lambda_2\mu_{hnf}}{1+\lambda_1}\frac{\partial^3 u}{\partial t^*\partial y^{*2}} + g(\rho\beta)_{hnf}\left(T^* - T_0\right), \qquad \ldots(2)$$

$$(\rho C_p)_{hnf}\frac{\partial T^*}{\partial t^*} = K_{hnf}\frac{\partial^2 T^*}{\partial y^{*2}} + \frac{\mu_{hnf}}{1+\lambda_1}\left(\frac{\partial u^*}{\partial y^*}\right)^2 - \frac{\partial q_r}{\partial y^*} + Q_0\left(T^* - T_0\right) + \sigma_{hnf}B_0^{\,2}u^{*2}, \qquad \ldots(3)$$

where u^* is component of velocity along the x^*-direction, temperature of hybrid nanofluid (T^*), electrical conductivity of the hybrid nanofluid (σ_{hnf}), density of hybrid nanofluid (ρ_{hnf}), dynamic viscosity of the hybrid nanofluid (μ_{hnf}), material parameters of Jeffrey fluid (λ_1 and λ_2), gravity of the hybrid nanofluid (g), radiative heat flux (q_r), effective specific heat of hybrid nanofluid ($(\rho C_p)_{hnf}$), thermal conductivity of hybrid nanofluid (K_{hnf}), thermal expansion of hybrid nanofluid (β_{hnf}).

The appropriate boundary conditions are

$$\text{At } y^* = 0 \Rightarrow u^* = 0,\ T^* = T_0,$$

$$-\frac{\partial P}{\partial x} = 1 + \varepsilon e^{it}, \qquad \ldots(4)$$

$$\text{At } y^* = h \Rightarrow u^* = 0,\ T^* = T_1. \qquad \ldots(5)$$

The effective physical properties of nanofluid and hybrid nanofluid are given as[15,44]

$$\left.\begin{aligned}
&\mu_{nf} = \frac{\mu_f}{(1-\phi)^{2.5}};\ \rho_{nf} = (1-\phi)\rho_f + \phi\rho_s;\\
&(\rho C_p)_{nf} = (1-\phi)(\rho C_p)_f + \phi(\rho C_p)_s;\\
&\frac{K_{nf}}{K_f} = \frac{K_s + 2K_f - 2\phi(K_f - K_s)}{K_s + 2K_f + \phi(K_f - K_s)};\\
&\frac{\sigma_{nf}}{\sigma_f} = 1 + \frac{3\left(\frac{\sigma_s}{\sigma_f} - 1\right)\phi}{\left(\frac{\sigma_s}{\sigma_f} + 2\right) - \left(\frac{\sigma_s}{\sigma_f} - 1\right)\phi};\\
&\beta_{nf} = (1-\phi)\beta_f + \phi\beta_s.
\end{aligned}\right\} \qquad \ldots(6)$$

$$\left.\begin{aligned}
&(\rho C_p)_{hnf} = (1-\phi)(\rho C_p)_f + \phi_{Au}(\rho C_p)_{Au} + \phi_{Al_2O_3}(\rho C_p)_{Al_2O_3};\\
&\frac{K_{hnf}}{K_f} = \frac{\left(\frac{\phi_{Au}K_{Au} + \phi_{Al_2O_3}K_{Al_2O_3}}{\phi}\right) + 2K_f + 2\left(\phi_{Au}K_{Au} + \phi_{Al_2O_3}K_{Al_2O_3}\right) - 2\phi K_f}{\left(\frac{\phi_{Au}K_{Au} + \phi_{Al_2O_3}K_{Al_2O_3}}{\phi}\right) + 2K_f - \left(\phi_{Au}K_{Au} + \phi_{Al_2O_3}K_{Al_2O_3}\right) + \phi K_f};\\
&\frac{\sigma_{hnf}}{\sigma_f} = 1 + \frac{3\left(\frac{\phi_{Au}\sigma_{Au} + \phi_{Al_2O_3}\sigma_{Al_2O_3}}{\sigma_f} - \phi\right)}{\left(\frac{\phi_{Au}\sigma_{Au} + \phi_{Al_2O_3}\sigma_{Al_2O_3}}{\phi\sigma_f} + 2\right) - \left(\frac{\phi_{Au}\sigma_{Au} + \phi_{Al_2O_3}\sigma_{Al_2O_3}}{\sigma_f} - \phi\right)};\\
&\beta_{hnf} = (1-\phi)\beta_f + \phi_{Au}\beta_{Au} + \phi_{Al_2O_3}\beta_{Al_2O_3}.
\end{aligned}\right\} \qquad \ldots(7)$$

Here $\phi = \phi_{Au} + \phi_{Al_2O_3}$, ϕ_{Au} is the volume fraction of gold nanoparticles, $\phi_{Al_2O_3}$ is the volume fraction of alumina nanoparticles.

By applying the Rosseland estimation for q_r and following [5,16,28] Eq. (3) becomes

$$\frac{\partial T^*}{\partial t^*} = \frac{K_{hnf}}{(\rho C_p)_{hnf}}\frac{\partial^2 T^*}{\partial y^{*2}} + \frac{\mu_{hnf}}{(\rho C_p)_{hnf}}\frac{1}{1+\lambda_1}\left(\frac{\partial u^*}{\partial y^*}\right)^2 + \frac{1}{(\rho C_p)_{hnf}}\left[\frac{16\sigma^*}{3\chi}T_0^3\frac{\partial^2 T^*}{\partial y^{*2}}\right] + \frac{\sigma_{hnf}B_0^{\,2}u^{*2}}{(\rho C_p)_{hnf}}$$

$$+\frac{Q_0}{(\rho C_p)_{hnf}}\left(T^*-T_0\right), \quad \ldots(8)$$

here, the Stephen-Boltzmann constant is σ^* and is the Rosseland mean absorption coefficient is χ .

Now, by following the dimensionless parameters and variables,

$$P=\frac{P^*}{A\rho_f h},\ u=\frac{u^*\omega}{A},\ x=\frac{x^*}{h},\ y=\frac{y^*}{h},\ t=t^*\omega,\ \theta=\frac{T^*-T_0}{T_1-T_0}$$

$\ldots(9)$

Eqs. (1), (2), and (8) become $\ldots(10)$

$$H^2\frac{\partial u}{\partial t}=-\frac{H^2}{A_1}\frac{\partial P}{\partial x}+\frac{A_2}{A_1}\frac{1}{1+\lambda_1}\frac{\partial^2 u}{\partial y^2}+\frac{A_2}{A_1}\frac{\lambda}{1+\lambda_1}\frac{\partial^3 u}{\partial t\partial y^2}-\frac{A_5}{A_1}M^2u+A_6\frac{Gr}{\mathrm{Re}}\theta,$$

...(11)

$$H^2\frac{\partial \theta}{\partial t}=\left(\frac{A_4}{A_3}+\frac{4}{3}\frac{Rd}{A_3}\right)\frac{1}{Pr}\frac{\partial^2\theta}{\partial y^2}+\frac{A_5}{A_3}EcM^2u^2+\frac{A_2}{A_3}\frac{1}{1+\lambda_1}\left(\frac{\partial u}{\partial y}\right)^2Ec+\frac{Q}{A_3}\theta.$$

$\ldots(12)$

Where $A_1=(1-\phi)+\phi_{Au}\frac{\rho_{Au}}{\rho_f}+\phi_{Al_2O_3}\frac{\rho_{Al_2O_3}}{\rho_f}$,

$$A_3=(1-\phi)+\phi_{Au}\frac{(\rho C_p)_{Au}}{(\rho C_p)_f}+\phi_{Al_2O_3}\frac{(\rho C_p)_{Al_2O_3}}{(\rho C_p)_f},$$

$$A_4=\frac{\left(\begin{array}{l}\left(\frac{\phi_{Au}K_{Au}+\phi_{Al_2O_3}K_{Al_2O_3}}{\phi}\right)+2K_f\\+2\left(\phi_{Au}K_{Au}+\phi_{Al_2O_3}K_{Al_2O_3}\right)-2\phi K_f\end{array}\right)}{\left(\begin{array}{l}\left(\frac{\phi_{Au}K_{Au}+\phi_{Al_2O_3}K_{Al_2O_3}}{\phi}\right)+2K_f\\-\left(\phi_{Au}K_{Au}+\phi_{Al_2O_3}K_{Al_2O_3}\right)+\phi K_f\end{array}\right)},$$

$$A_5=1+\frac{\left(3\left(\frac{\phi_{Au}\sigma_{Au}+\phi_{Al_2O_3}\sigma_{Al_2O_3}}{\sigma_f}-\phi\right)\right)}{\left(\begin{array}{l}\left(\frac{\phi_{Au}\sigma_{Au}+\phi_{Al_2O_3}\sigma_{Al_2O_3}}{\phi\sigma_f}+2\right)\\-\left(\frac{\phi_{Au}\sigma_{Au}+\phi_{Al_2O_3}\sigma_{Al_2O_3}}{\sigma_f}-\phi\right)\end{array}\right)},$$

$A_2=\frac{\mu_f}{(1-\phi)^{2.5}}$, $A_6=(1-\phi)+\phi_{Au}\frac{\beta_{Au}}{\beta_f}+\phi_{Al_2O_3}\frac{\beta_{Al_2O_3}}{\beta_f}$,

$\mathrm{Pr}=\frac{(\rho C_p)_f\nu_f}{K_f}$ is the Prandtl number,

$Gr=\frac{g\beta_f\left(T_1-T_0\right)h^3}{\nu_f^2}$ is the Grashof number,

$Rd=\frac{4\sigma^*T_1^3}{K_f\chi}$ is the radiation parameter, $M=B_0h\sqrt{\frac{\sigma_f}{\mu_f}}$ is the Hartmann number, $H=h\sqrt{\frac{\omega}{\nu_f}}$ is the frequency parameter, $\lambda=\lambda_2\omega$ is the dimensionless material parameter, $Ec=\frac{A^2}{\omega^2\left(C_p\right)_f(T_1-T_0)}$ is the Eckert number, $Q=\frac{Q_0h^2}{\left(\rho C_p\right)_f\nu_f}$ is the heat source/sink parameter, $\mathrm{Re}=\frac{Ah}{\omega\nu_f}$ is Reynolds number.

The corresponding boundary conditions are

$$u(0)=0,\ \theta(0)=0, \quad \ldots(13)$$

$$u(1)=0,\ \theta(1)=1. \quad \ldots(14)$$

Solution Methodology

On account of Eq. (10), the velocity and temperature can be conveyed as follows:

$$u(y,t)=u_0\left(y\right)+\varepsilon u_1(y)e^{it} \quad \ldots(15)$$

$$\theta(y,t)=\theta_0\left(y\right)+\varepsilon\theta_1(y)e^{it} \quad \ldots(16)$$

Using Eqs. (10), (15), and (16) in Eqs. (11)-(12) and then likening the appropriate coefficient of same powers of ε, we obtain

$$\frac{A_2}{1+\lambda_1}u_0^{''}\left(y\right)-A_5M^2u_0\left(y\right)+A_6A_1\frac{Gr}{\mathrm{Re}}\theta_0+H^2=0, \quad \ldots(17)$$

$$\left(\frac{A_2}{1+\lambda_1}+\frac{A_2\lambda i}{1+\lambda_1}\right)u_1^{''}\left(y\right)-\left(A_5M^2+A_1iH^2\right)u_1\left(y\right)+A_6A_1\frac{Gr}{\mathrm{Re}}\theta_1+H^2=0,$$

$\ldots(18)$

$$\left(A_4+\frac{4}{3}Rd\right)\frac{1}{Pr}\theta_0''(y)+\frac{A_2}{1+\lambda_1}Ecu_0'^2(y)+A_5M^2Ecu_0^2(y)+Q\theta_0=0, \quad \ldots(19)$$

$$\left(A_4+\frac{4}{3}Rd\right)\frac{1}{Pr}\theta_1''(y)+\left(Q-A_3iH^2\right)\theta_1(y)+\frac{A_2}{1+\lambda_1}Ec2u_0'(y)u_1'(y)$$

$$+A_5 2M^2Ecu_0(y)u_1(y)=0. \quad \ldots(20)$$

The appropriate boundary conditions are

$$\left.\begin{aligned}u_0(0)=0,\ \theta_0(0)=0\\ u_1(0)=0,\ \theta_1(0)=0\end{aligned}\right\}, \quad \ldots(21)$$

$$\left.\begin{aligned}u_0(1)=0,\ \theta_0(1)=1\\ u_1(1)=0,\ \theta_1(1)=0\end{aligned}\right\}. \quad \ldots(22)$$

Now, the dimensionless Nusselt number at the walls for the present study is expressed as [2, 24, 40]

$$Nu=\left(A_4+\frac{4}{3}Rd\right)\left(\frac{d\theta_0}{dy}+\varepsilon e^{it}\frac{d\theta_1}{dy}\right)_{y=0,1} \quad \ldots(23)$$

Eqs. (17)-(20) are solved by utilizing the shooting technique with the Runge-Kutta fourth-order procedure with boundary conditions (21) and (22). The step size $0.001\left(\Delta y=0.001\right).1\times10^{-10}$ exactness is determined for the convergence criteria. Flow chart of solution methodology is given in Fig. 2.

Numerical solution

$$f_2'=\frac{1+\lambda_1}{A_2}\left(A_5M^2f_1-A_6A_1\frac{Gr}{\mathrm{Re}}f_5-H^2\right),$$

$$f_4'=\frac{1+\lambda_1}{A_2(1+\lambda i)}\left(\left(A_5M^2+A_1iH^2\right)f_3-A_6A_1\frac{Gr}{\mathrm{Re}}f_7-H^2\right),$$

$$f_6'=\frac{1}{\left(A_4+\frac{4}{3}Rd\right)\frac{1}{Pr}}\left(-\frac{A_2}{1+\lambda_1}Ecf_2^2-A_5M^2Ecf_1^2-Qf_5\right),$$

$$f_8'=\frac{1}{\left(A_4+\frac{4}{3}Rd\right)\frac{1}{Pr}}\left(-\left(Q-A_3iH^2\right)f_7-\frac{A_2}{1+\lambda_1}2Ecf_2f_4-2A_5M^2Ecf_1f_3\right)$$

Here,

$$u_0=f_1,u_0'=f_2,u_1=f_3,u_1'=f_4,\theta_0=f_5,\theta_0'=f_6,\theta_1=f_7,\theta_1'=f_8.$$

Entropy generation

The dimensional form of the entropy generation of the present work is given as [37, 38]

$$SG=\frac{K_f}{T_0^2}\left(\frac{K_{hnk}}{K_f}+\frac{16\sigma^*T_0^3}{3K_f\chi}\right)\left(\frac{\partial T^*}{\partial y^*}\right)^2+\frac{\mu_{hnf}}{(1+\lambda_1)T_0}\left(\frac{\partial u^*}{\partial y^*}\right)^2+\frac{\sigma_{hnf}B_0^2}{T_0}u^{*2} \quad \ldots(24)$$

The non-dimensional form of entropy generation is

$$NG=\left(A_4+\frac{4Rd}{3}\right)\left(\frac{\partial\theta}{\partial y}\right)^2+\frac{A_2Ec\,\mathrm{Pr}}{(1+\lambda_1)\alpha_1}\left(\frac{\partial u}{\partial y}\right)^2+\frac{A_5M^2Ec\,\mathrm{Pr}}{\alpha_1}(u)^2. \quad \ldots(25)$$

Where $NG=\dfrac{SGT_0^2h^2}{K_f\left(T_1-T_0\right)^2}$ is the entropy generation, $\alpha_1=\dfrac{T_1-T_0}{T_0}$ is the temperature difference

Bejan number is defined as

Bejan number $(Be)=$

$$\frac{Entropy\ generation\ due\ to\ heat\ and\ Mass\ transfer}{Total\ entropy\ generation}$$

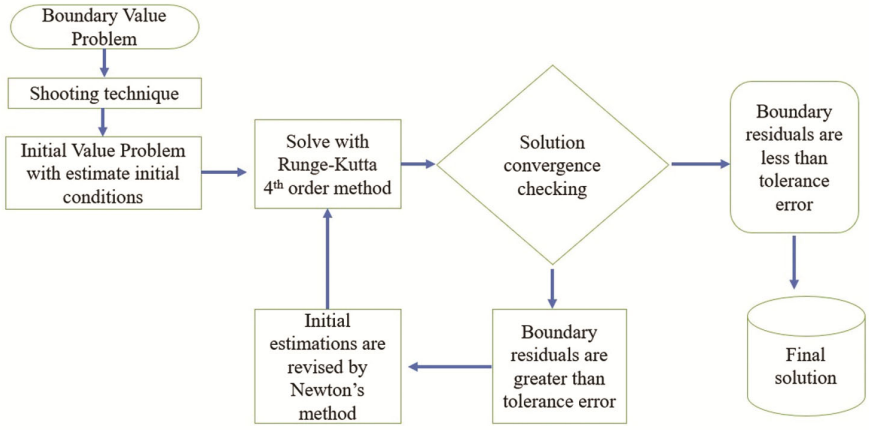

Fig. 2 — Flow chart of solution methodology

$$Be = \frac{\left(A_4 + \frac{4Rd}{3}\right)\left(\frac{\partial\theta}{\partial y}\right)^2}{NG}. \qquad \ldots(26)$$

Table 2 — Comparison of the present study with the results provided by NDSolve of θ' at left wall, when $H = 1$, $M = 2$, $\lambda = \lambda_1 = 0.5$, $Ec = 0.5$, $\Pr = 21$, $t = \frac{\pi}{4}$, $Q = -1$, $Gr = 1$, $\mathrm{Re} = 2$, $Rd = 1$

Parameter	Values	$\theta_{y=0}$	
		Present scheme	ND Solve
λ_1	1.0	0.908559	0.908566
	2.0	1.031268	1.031268
	3.0	1.130308	1.130308
Ec	0.1	0.517254	0.517254
	0.3	0.662208	0.662207
	0.6	0.930127	0.930133
M	0.5	1.201302	1.201308
	1.0	1.088754	1.088759
	1.5	0.953712	0.953714
Gr	0.1	0.569850	0.569850
	0.2	0.588126	0.588126
	0.3	0.608427	0.608426

The comparative result shows that there is an excellent agreement between the current outcomes and outcomes provided by NDSolve utilizing MATHEMATICA which is prearranged in Table 2.

Results and Discussion

The objective of the current study illustrates the effect of emerging physical parameters on the velocity, temperature, entropy generation, and Bejan number profiles of Jeffrey hybrid nanofluid with the help of pictographic results as exhibited in Figs. 3-8. In this study u_s, u_t, θ_s, θ_t denote the steady velocity, unsteady velocity, steady temperature, and unsteady temperature, respectively. During the study, the values of pertinent parameters are respectively fixed as H=1, M=1, $\lambda = \lambda_1 = 0.5$, $Ec = 0.5$, $\Pr = 21$, $t = \pi/3$, $Q = -1$, Gr=1, $\mathrm{Re} = 2$, Rd=2. Unless otherwise stated.Figs. 3(a)-3(d) elucidate the influences of Hartmann number (M), frequency parameter (H). Grashof number (Gr) material parameter (λ_1), on u_s. Fig. 3(a) illustrates that the increment in M lowers the steady velocity. Physically the applied magnetic field creates a resistive force that reacts in

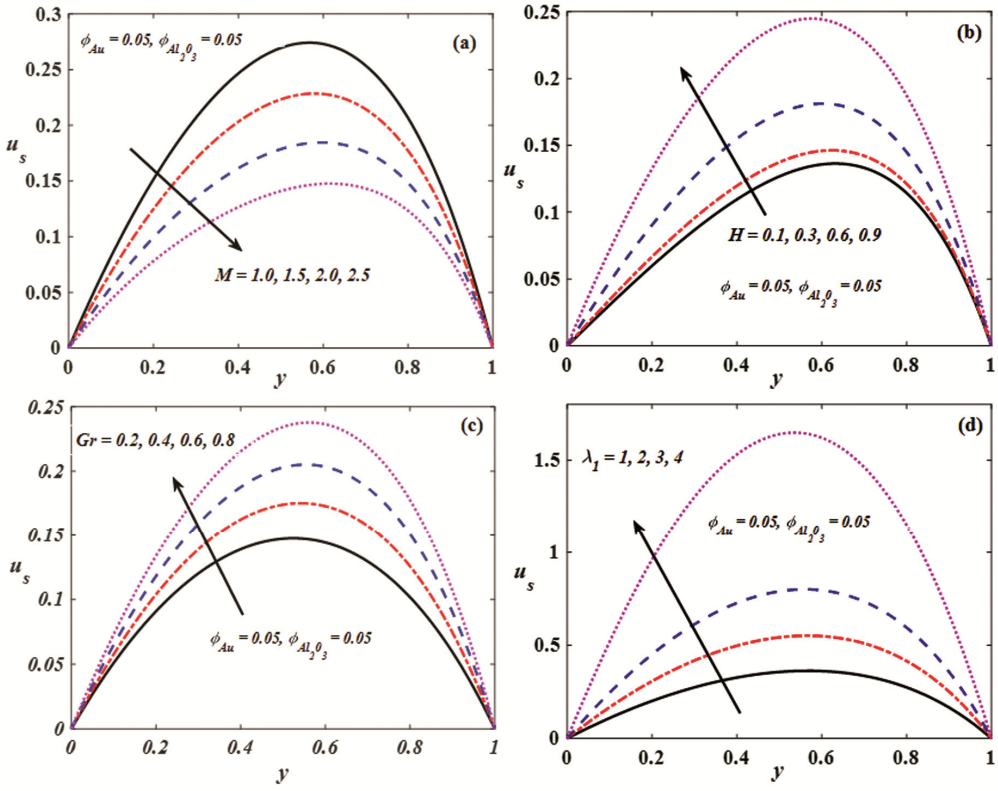

Fig. 3 — Steady velocity dispersion (a) consequence of $M = 1.0, 1.5, 2.0, 2.5$, (b) consequence of $H = 0.1, 0.3, 0.6, 0.9$, (c) consequence of $Gr = 0.2, 0.4, 0.6, 0.8$ and (d) effect of $\lambda_1 = 1, 2, 3, 4$

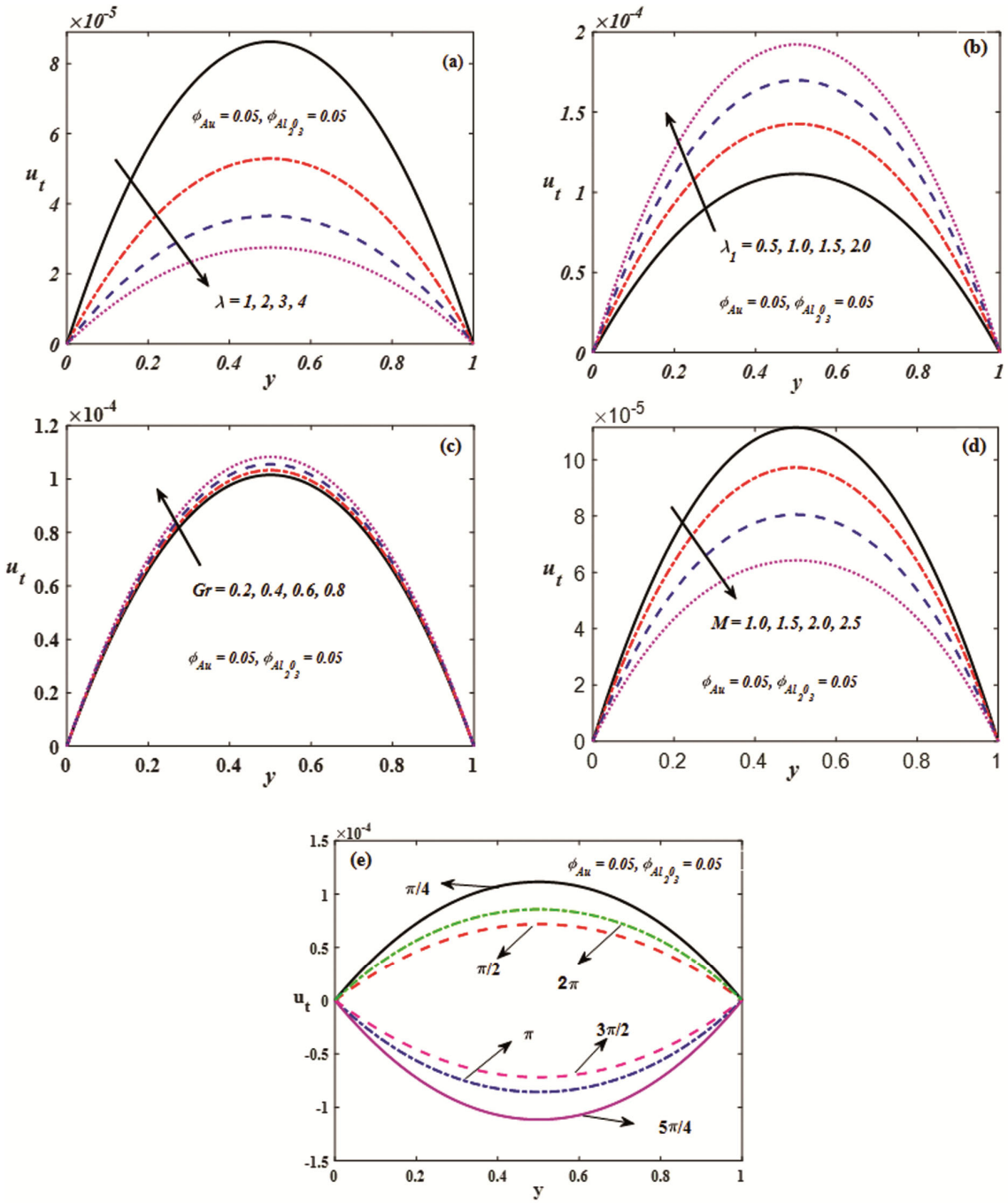

Fig. 4 — Unsteady velocity dispersion (a) consequence of $\lambda = 1, 2, 3, 4$, (b) consequence of $\lambda_1 = 0.5, 1.0, 1.5, 2.0$, (c) consequence of $Gr = 0.2, 0.4, 0.6, 0.8$, (d) consequence of $M = 1.0, 1.5, 2.0, 2.5$, and (e) consequence of $t = \frac{\pi}{4}, \frac{\pi}{2}, \pi, \frac{5\pi}{4}, \frac{3\pi}{2}, 2\pi$

the opposite direction of the flow-field as well as hybrid nanoparticles which can be seen as a reduction of the velocity of hybrid nanofluids. The reverse behaviour is observed by varying frequency parameter (see fig. 3(b)). Fig. 3(c) elucidates that velocity is increased due to enhancing the Grashof number. Because the Grasof number is directly related to the bouncy force. Subject to an increment in Gr as the predicted velocity rises. The similar trend is switched on for material parameter (see fig. 3(d)).

Figs. 4(a)-4(e) deliberate the impacts of material parameters (λ, λ_1), Grashof number (Gr), Hartmann

number (M), and time (t) on u_t. Fig. 4(a) gives the impact of λ on unsteady velocity of the hybrid nanofluid. It illustrates that an increment in λ decrease unsteady velocity. The reverse nature is depicted in Fig. 4(b) by varying λ_1. Fig. 4(c) elucidates that the enhancement in Gr increases the unsteady velocity of the hybrid nanofluid. Fig. 4(d) portrays that intensifying M slows the movement of the fluid. From Fig. 4(e) it is clearly observed that the unsteady velocity is oscillating due to varying the values of time (t).

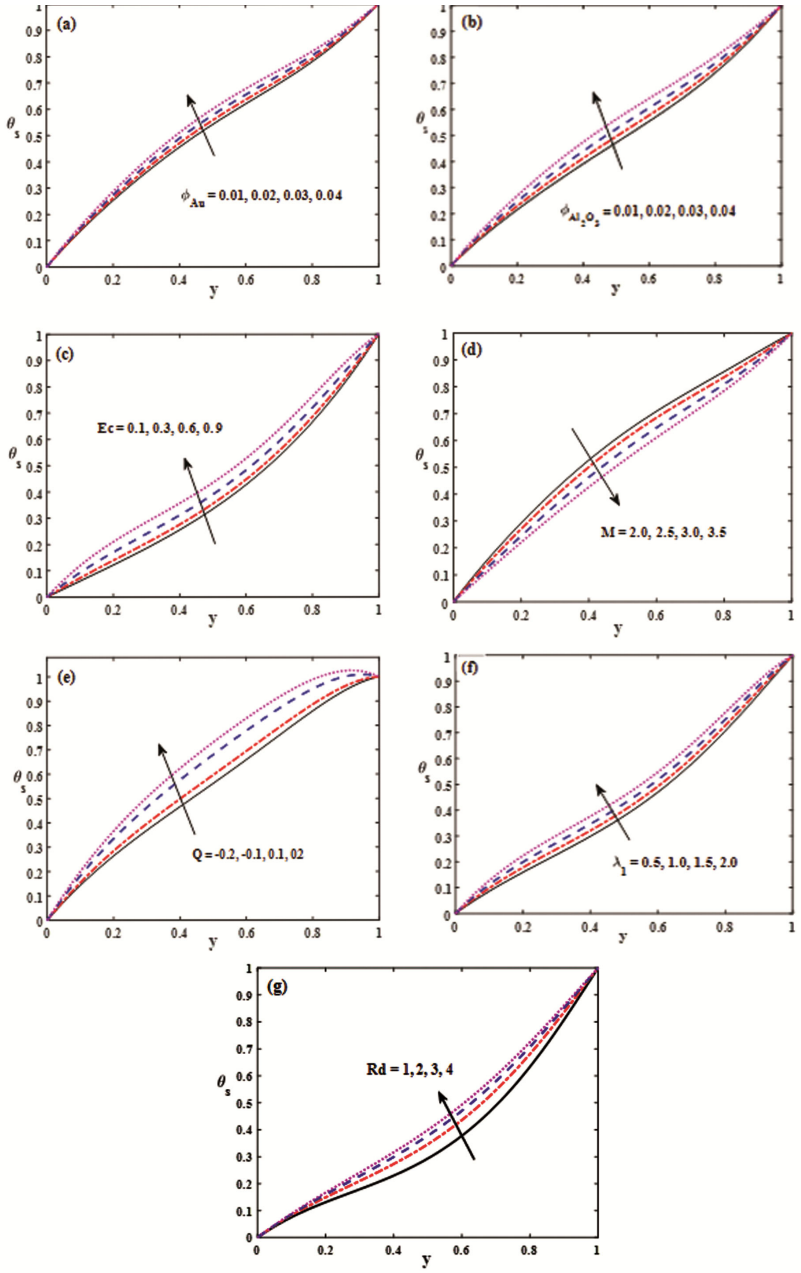

Fig. 5 — Steady temperature dispersion (a) consequence of $\phi_{Au} = 0.01, 0.02, 0.03, 0.04$ when $\phi_{Al_2O_3} = 0.05$, (b) consequence of $\phi_{Al_2O_3} = 0.01, 0.02, 0.03, 0.04$ when $\phi_{Au} = 0.05$, (c) consequence of $Ec = 0.1, 0.3, 0.6, 0.9$, (d) consequence of $M = 2.0, 2.5, 3.0, 3.5$ when $H = 1.5$, (e) consequence of $Q = -0.2, -0.1, 0.1, 0.2$, (f) consequence of $\lambda_1 = 0.5, 1.0, 1.5, 2.0$ and (g) consequence of $Rd = 1, 2, 3, 4$

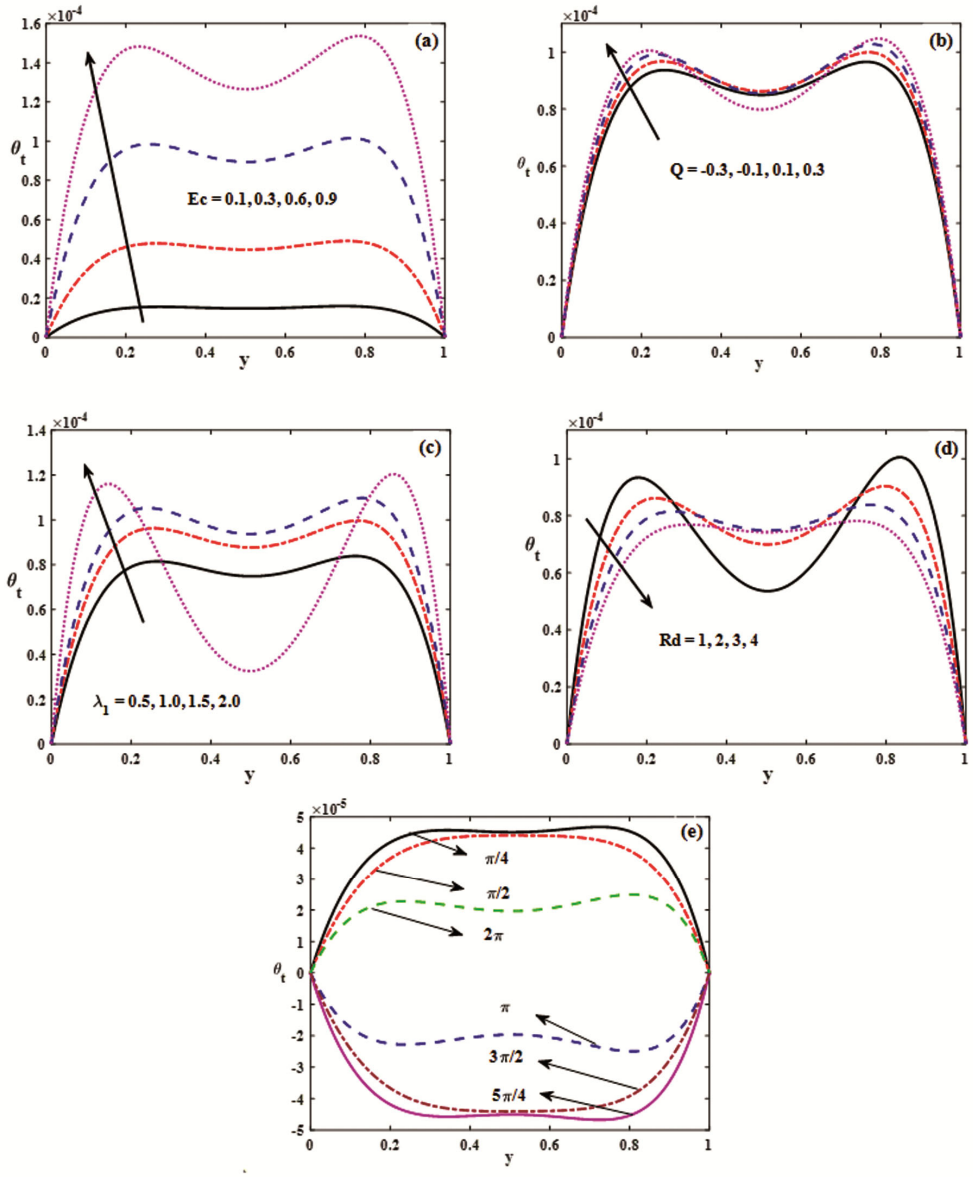

Fig. 6 — Unsteady temperature dispersion when $H=1.5$ (a) consequence of $Ec=0.1,0.3,0.6,0.9$, (b) consequence of $Q=-0.3,-0.1,0.1,0.3$, (c) consequence of $\lambda_1=0.5,1.0,1.5,2.0$, (d) consequence of $Rd=1,2,3,4$, (e) consequence of $t=\frac{\pi}{4},\frac{\pi}{2},\pi,\frac{5\pi}{4},\frac{3\pi}{2},2\pi$

Figs 5(a)-(g) elucidate the impressions of ϕ_{Au}, $\phi_{Al_2O_3}$, Ec, M, Q, λ_1, Rd on steady temperature. From Fig. 5(a) and fig. 5(b), one can infer that the temperature of the hybrid nanofluid increasing with increasing ϕ_{Au} and $\phi_{Al_2O_3}$, because a large amount of nanoparticles in the fluid makes it highly conductive. As a result, the fluid's temperature increases. Fig. 5(c) shows the effect of Ec on steady temperature of the hybrid nanofluid. It converts kinetic energy into internal energy by opposing the stresses on viscous fluids. Increasing Ec increases internal energy, which increases the fluid temperature. The reverse nature observed from fig. 5(d) by varying M. Fig. 5(e) illustrates that the increment in heat sink decreases the temperature whereas the opposite behaviour can be noticed in temperature for the increment in heat source. The same trend is switched on for λ_1 (see fig.

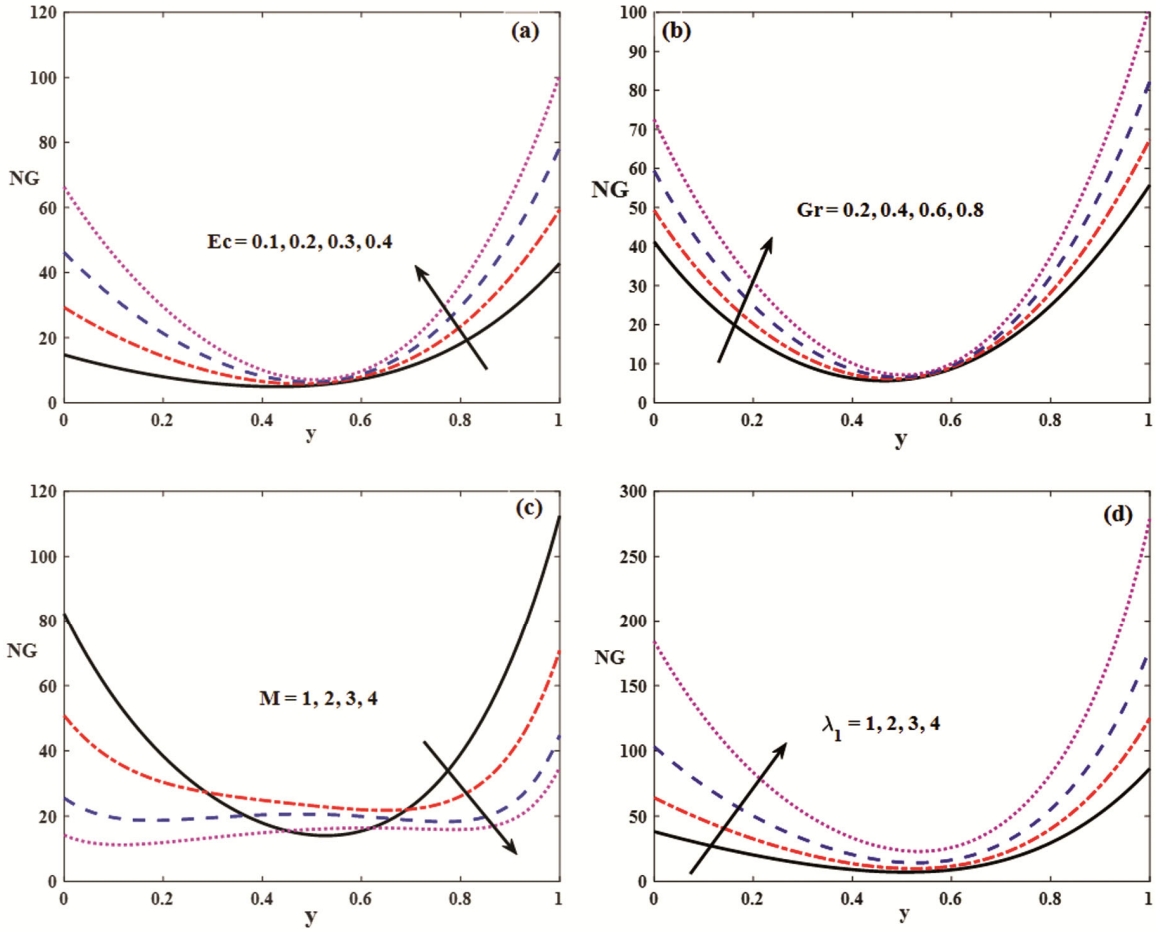

Fig. 7 — Entropy dispersion (a) consequence of $Ec = 0.1, 0.2, 0.3, 0.4$, (b) consequence of $Gr = 0.2, 0.4, 0.6, 0.8$, (c) consequence of $M = 1, 2, 3, 4$, and (d) consequence of $\lambda_1 = 1, 2, 3, 4$

5(f)). Fig. 5(g) demonstrates that there is an increase in temperature with a rise in Rd. Physically, the radiation parameters indicate the relative contribution of conduction and radiation to heat transfer. It is obvious that as the radiation parameter rises, the temperature rises as well.

Figs. 6(a)-6(e) exhibit the influences of Ec, Q, λ_1, Rd, and t on θ_t of the hybrid nanofluid profile (θ_t). Fig. 6(a) portrays that the unsteady temperature is increasing and wavering with an enhancement of *Ec*. Figs. 6(b) and 6(c) demonstrates that the unsteady temperature profile displays increasing near the walls and oscillating at the center of the walls as the increment of Q and λ_1. Fig. 6(d) demonstrates that unsteady temperature is declining with an enhancement of Rd and also it displays that θ_t profiles show the wavering behaviour. Fig. 6(e) demonstrates that the unsteady temperature is wavering for different values of time (t).

Figs 7(a)-7(d) indicate the impacts of Eckert number, Grashof number, Hartmann number, and material parameter on entropy generation (NG) profiles. Fig. 7(a) displays that the entropy generation is upsurged for higher values of Eckert number. In the case of high Eckert numbers, the entropy generation is boosted by the fact that kinetic energy dominates the enthalpy difference. As a result, the entropy generation is increased. A similar nature is observed by varying Grashof number (see Fig. 7(b)). Fig. 7(c) presents that the entropy generation is reduced for higher values of M. Consequently, the thermal boundary layer is diminished for the reason that the retarding forces created by the applied magnetic field. The opposite nature is noticed by varying material parameter (see fig. 7(d)). Figs 8(a)-8(b) elucidate the influences of M and Ec on Bejan number of Jeffrey hybrid nanofluid. Fig 8(a) demonstrates that the

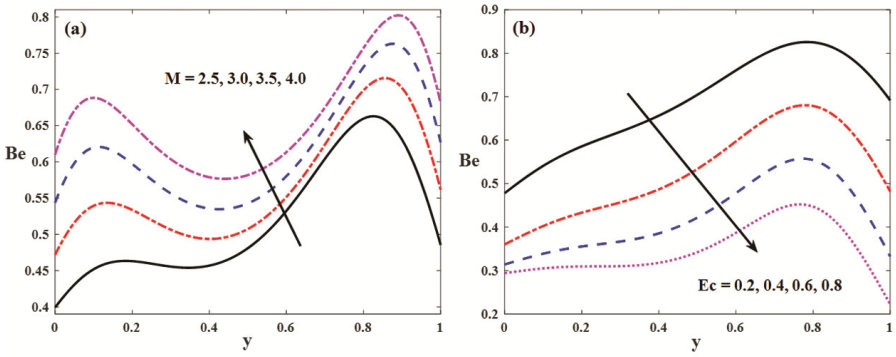

Fig. 8 — Bejan number dispersion (a) consequence of $M = 2.5, 3.0, 3.5, 4.0$ and (b) consequence of $Ec = 0.2, 0.4, 0.6, 0.8$

Table 3 — Variations of heat transfer rate at the left wall for various values of λ_1, Ec, Rd, at $H = 1$, $M = 0.5$, $\lambda = \lambda_1 = 0.5$, $Ec = 0.5$, Pr = 21, $t = \frac{\pi}{4}$, $Q = -1$, $Gr = 1$, Re = 2, $Rd = 3$

parameter	value	*Nu*		
		Base fluid (Blood)	Au-Blood	Au-Al_2O_3/Blood
Ec	0.1	2.824379	2.992268	3.331345
	0.3	3.106424	3.351305	4.139638
	0.6	3.534917	3.909396	5.580979
λ_1	0.5	3.391346	3.720673	5.064529
	1.0	3.617746	4.017722	5.898584
	1.5	3.839882	4.313515	6.834499
M	1.0	3.310927	3.607596	4.778070
	1.5	3.210586	3.469668	4.429272
	2.0	3.113849	3.340203	4.107732
Rd	1.0	1.280529	1.494299	2.405499
	2.0	2.274160	2.557505	3.728301
	3.0	3.391346	3.720673	5.064529

influence of Hartmann number on Bejan number (Be). It can be seen that the acceleration in the Bejan number is caused by the escalating Hartmann number because a higher resistance is acting on fluid flow. The opposite nature is observed by varying Ec (see fig. 8(b)).

The Nusselt number at the left wall (y=0) for different values of Ec, λ_1, M and Rd are presented in Table 3. It indicates that the heat transfer rate at the left wall is enhanced while increasing the Eckert number, material parameter, and radiation parameter. This table shows that the heat transfer rate is a decreasing function of Hartmann number. It is clearly observed that, when Ec increases from 0.1 to 0.6, there is an increment of 25.1%, 30.6%, and 67.5% in the heat transfer rate of base fluid, mono nanofluid, and hybrid nanofluid respectively. Furthermore, it is noticed that there is a 5.9% decline in the heat transfer rate of base fluid, 7.4% dwindle in the case of mono nanofluid and 14% diminish in the case of hybrid nanofluid when Hartmann number increases from 1 to 2. At $Ec = 0.3$, when we add Au nanoparticles (mono nanouid case) to the base fluid then there is 7.8% rise in heat transfer rate while there is 23.5% increment in heat transfer rate by adding Au and Al_2O_3 nanoparticles (hybrid nanouid case) to the base fluid. Also, this table shows that a mono nanofluid has a higher heat transfer rate than a conventional liquid (base fluid) whereas the hybrid nanofluids have a greater heat transfer capacity than mono nanofluids.

Conclusion

The present study deals with the entropy analysis on pulsatile flow of Jeffrey hybrid nanofluid through a vertical channel with Ohmic heating, thermal radiation, and heat source/sink effects. The

transformation of the governing equations into a system of ordinary differential equations are made by applying the perturbation procedure and then numerically tackled through the fourth-order Runge-Kutta scheme aided by the shooting technique. The influence of various pertinent parameters and variables on velocity, temperature, entropy generation, and Bejan number are presented graphically. Nusselt number distributions for various physical parameter values are tabulated and discussed in detail. The main outcomes are

- The temperatures are rising functions by mounting the Ec and Rd.
- The Nusselt number is magnifying for rising values of material parameter and Eckert number whereas the opposite nature can be identified with an increment in Hartmann number at the left wall.
- The entropy generation is increasing for intensifying Ec, and Rd whereas the reverse nature can be found for uplifting values of M.
- Bejan number is dwindling for escalating viscous dissipation whereas it is increasing with the enhancement in Hartmann number.

References

1 Wang C, *ASME J Appl Mech*, 38 (1971) 553.
2 Radhakrishnamacharya G & Maiti M K, *Int J Heat Mass Transfer*, 20 (1977) 171.
3 Makinde O D, *Int Commun Heat Mass Transfer*, 32 (2005) 1411.
4 Eid M R, Al-Hossainy A F & Zoromba M S, *Commun Theo Phys*, 71 (2019) 1425.
5 Adesanya S O, Falade J A & Makinde O D, *UPB Sci Bull Ser D*, 77 (2015) 36.
6 Ali K & Abdon A J, *Therm Anal Calorim*, 146 (2021) 689.
7 Govindarajulu K & Reddy A S, *Phys Fluids*, 34 (2022) 013105.
8 Mamatha S U, Devi R R, Ahammad N A, Shah N A, Rao B M, Raju C S K & Guedri K, *Int J Mod Phys B*, 37 (2023) 2350007.
9 Kot M A & Elmaboud Y A, *J Therm Anal Calorim*, 147 (2022) 4355.
10 Eldabe N T, *J Egypt Math Soc*, 25 (2017) 375.
11 Pant C S, Kishore P & Kumar S, *Int J Therm Sci*, 176 (2022) 107529.
12 Maskeen M M, Mehmood O U & Zeeshan A, *J Visual*, 21 (2018) 407.
13 Haq R U, Shahzad F & Al-Mdallal Q M, *Results Phys*, 7 (2017) 57.
14 Shah N A, Al-Zubaidi A & Saleem S, *Adv Math Phys*, 2021 (2021) 1.
15 Wang X, Qiao Y, Qi H & Xu H, *Int Commun Heat Mass Transfer*, 133 (2022) 105930.
16 Xu H & Sun Q, *Commun Theor Phys*, 71 (2019) 903.
17 Kumar P B & Suripeddi S, *Eur Phys J Spec Top*, 230 (2021) 1465.
18 Choi S U S & Eastman J, *Am Soc Mech Eng Fluids Eng Div*, 231 (1995) 99.
19 Devi S U & Devi S A, *J Nanofluids*, 36 (2017) 419.
20 Waini I, Ishak A, Groşan T & Pop I, *Int Commun Heat Mass Transfer*, 114 (2020) 104565.
21 Hayat T & Nadeem S, *Results Phys*, 7 (2017) 2317.
22 Thamizharasan T & Reddy A S, *Indian J Pure Appl Phys*, 60 (2022) 680.
23 Azimi M, Ganji D D, Azimi A & Riazi R, *Indian J Chem Technol*, 25 (2018) 281.
24 Manzoor N, Qasim I, Khan M I, Ahmed M W, Guedri K, Bafakeeh O T & Galal A M, *Appl Sci*, 12 (2022) 9737.
25 Bafakeeh O T, Raghunath K, Ali F, Khalid M, Tag-El D E S M, Oreijah M, Guedri K, Khedher N B & Khan M I, *J Catal*, 12 (2022) 1233.
26 Sehar B, Waris A, Gilani S O, Ansari U, Mushtaq S, Khan N B, Jameel M, Khan M I, Bafakeeh O T & Tag-El D E S M, *J Crystals*, 12 (2022) 1429.
27 Waqas H, Oreijah M, Guedri K, Khan S U, Yang S, Yasmin S, Khan M I, Bafakeeh O T, Tag-El E S M & Galal A M, *J Crystals*, 12 (2022) 1308.
28 Shahid M, Javed H M A, Ahmad M I, Qureshi A A, Khan M I, Alnuwaiser M A, Ahmed A, Khan M A, Tag-El D E S M, Shahid A & Rafique A, *Nanomater*, 12 (2022) 3413.
29 Kirankumar H V, Thejas R & Naveen C S, *Bioref*, 12 (2022) 11.
30 Li S, Puneeth V, Saeed A M, Singhal A, Al-Yarimi F A, Khan M I & Eldin S M, *Sci Rep*, 13 (2023) 2340.
31 Abbas S Z, Wang X, Khan W A, Hobiny A & Iqbal K J, *Energy Storage*, 51 (2022) 104462.
32 Ahmed M F, Zaib A, Ali F, Bafakeeh O T, Tag-El D E S M, Guedri K, Elattar S & Khan M I, *Micromachines*, 13 (2022) 1768.
33 Li S, Khan M I, Alzahrani F & Eldin S M, *Case Stud Therm Eng*, 26 (2021) 100975.
34 Abbasi A, Farooq W, Tag-El D E S M, Khan S U, Khan M I, Guedri K, Elattar S, Waqas M & Galal A M, *Micromachines*, 13 (2022) 1415.
35 Hussain S M, Sharma R & Chamkha A J, *Chinese J Phys*, 75 (2022) 120.
36 Iftikhar N, Rehman A & Sadaf H, *Int Commun Heat Mass Transf*, 120 (2021) 105012.
37 Elsaid E M & Abdel-Wahed M S, *Case Stud Therm Eng*, 25 (2021) 100913.
38 Hayat T, Ullah H, Ahmad B & Alhodaly M S, *Int Commun Heat Mass Trans*, 120 (2021) 104965.
39 Cheng L, Nawaz M, Kaneez H, Alaoui M K, Selmi A, Li C & Assilzadeh H, *Int Commun Heat Mass Transf*, 126 (2021) 105275.
40 Thamizharasan T & Reddy A S, *Eur Phys J Spec Top*, 231 (2022) 1205.
41 Rajkumar D, Subramanyam R A, Srinivas S & Jagadeshkumar K, *Int J Appl Comput Math*, 8 (2022) 1.
42 Nazeer M, Hussain F, Khan M I & Khalid K, *Waves Random Complex Media*, (2022) 1.
43 Saif R S, Muhammad T, Sadia H & Ellahi R, *Phys A Stat Mech Appl*, 551 (2020) 124060.
44 Aleem M, Asjad M I, Ahmadian A, Salimi M & Ferrara M, *Eur Phys J Plus*, 135 (2020) 1.
45 Ali A, Saleem S, Mumraiz S, Saleem A, Awais & Khan D N, *J Therm Anal Calorim*, 143 (2021) 1985.

46 Hafeez M, Hashim & Khan M, *Appl Nanosci*, 10 (2020) 5459.
47 Sáchica D, Treviño C & Martínez-Suástegui L, *Int J Heat Fluid Flow*, 86 (2020) 108713.
48 Salawu S O & Ogunseye H A, *Results Eng*, 5 (2020) 100072.
49 Falade J A, Adesanya S O, Ukaegbu J C & Osinowo M O, *Alexandria Eng J*, 55 (2016) 69.
50 Hayat T, Kainat Z, Khan S A & Alsaedi A, *Adv Mech Eng*, 14 (2022) 168781322210954.
51 Motsumi T G & Makinde O D, *Phys Scr*, 86 (2012) 045003.
52 Santhosh C, *Indian J Chem Technol*, 29 (2022) 311.
53 Hayat T, Kanwal M, Qayyum S & Alsaedi A, *Phys A Stat Mech App*, 544 (2020) 123437.
54 Mansour M A, Siddiqa S, Gorla R S R & Rashad A M, *Therm Sci Eng Prog*, 6 (2018) 57.
55 Javed M F, Waqas M, Khan M I, Khan, N B, Muhammad R, Rehman M, Khan S W & Hassan M T, *Appl Nanosci*, 10 (2020) 3011.
56 Li S, Khan M I, Alzahrani F & Eldin S M, *Case Stud Therm Eng*, 42 (2023) 102722.
57 Hussain S, Ahmed S E & Akbar T, *Int J Heat Mass Transf*, 114 (2017) 1054.